Comprehensive characterization of gold nanoparticles and their protein conjugates used as a label by hollow fiber flow field flow fractionation with photodiode array and fluorescence detectors and multiangle light scattering

Comprehensive characterization of gold nanoparticles and their protein conjugates used as a label by hollow fiber flow field flow fractionation with photodiode array and fluorescence detectors and multiangle light scattering

Valentina Marassi [a b], Donato Calabria [a], Ilaria Trozzi [a], Andrea Zattoni [a b], Pierluigi R eschiglian [a b], Barbara Roda [a b]

Journal of Chromatography A. Volume 1636, 11 January 2021, 461739

Comprehensive characterization of gold nanoparticles and their protein conjugates used as a label by hollow fiber flow field flow fractionation with UV, Fluorescence and MALS detector

Valentina Marassi[1,2], Donato Calabria[1], Ilaria Trozzi[1], Andrea Zattoni[1,2], Pierluigi Reschiglian[1,2], Barbara Roda[1,2,*]

[1]Department of chemistry G. Ciamician, University of Bologna, Italy
[2]byFlow srl, Bologna, Italy

[*]Corresponding author: barbara.roda@unibo.it

Highlights

- Development of NP probes for biosensors can benefit from integrated separation-characterization approach
- Miniaturized flow field flow fractionation-multidetection assists critical steps of nanoparticle-antibody conjugation
- Unreacted conjugants are easily recovered
- Antibody-nanoparticle size and stability is investigated

Abstract

Most of lateral flow immunoassay (LFIA) devices rely on gold nanoparticles (GNP) labeled antibodies or other biospecific proteins, to achieve reagent-less color-based detection. GNP size, GNP-protein conjugation level and its stability are crucial points for the development of precise and accurate methods. In addition, the purification of the GNP-protein conjugates from unreacted protein and GNP, is necessary for adequate analytical performance of the assay.

To assist the synthesis and production process of GNP and their protein conjugates, we use for the first time a non-destructive, particle separation-multi-detection approach based on miniaturized flow field flow fractionation (HF5). A separation method was developed to baseline size-separate GNP, GNP-protein, protein and GNP including BSA used as a surface coater in less than 30 minutes.

Freshly synthesized GNP were first characterized and then conjugated with two different model antibodies: a mouse immunoglobulin (IgG) and a fluorescein-labeled mouse immunoglobulin (FITC-IgG).

The IgG-GNP complexes were fractionated using the HF5 apparatus, able to separate IgG-GNP from free proteins by their hydrodynamic size, allowing purification of the conjugation product. Both IgG-GNPs and GNPs were characterized according to their size by the MALS detector, and according to their Surface Plasmon Resonance and spectrum by UV-Vis detection, improving the results obtained via batch characterization.

This simple non-invasive approach is very useful for the LFIA development and optimization: the use of HF5-mutidetection offers a unique tool for this purpose facilitating the industrialization of the process and the relate optimization and standardization.

1. Introduction

The synthesis and characterization of new nanomaterials are fundamental for the development of innovative biomedical diagnostic devices and therapeutic agents [1,2]. Gold nanoparticles (GNPs) are versatile nanomaterials of extraordinary interest, attributable to their peculiar size-related optical properties, in particular for the strong light absorption associated with surface plasmon resonance phenomenon, which is used as a sensitive probe in the biomedical field, from biosensing to *in vivo* imaging in cancer treatment and drug delivery [3,4].

The more common use of GNPs is as a label in reagent-less paper-based assay and particularly lateral flow immunoassay (LFIA) since the first development of the widely used pregnancy test. The unique optical properties of GNP arise from the formation of a strong red-colored band in LFIA caused by the increased concentration of the GNPs labelled Ab interacting with the analyte in the test line while is uncoloured when dispersed in the immunocromatographic pad.

GNP can also be employed as beads for antibody immobilisation prior to deposition on a solid support. This approach improves immunoassay performance, since the antibody is not directly linked to plastic or paper. It can be more efficiently deposited on selected surfaces, increasing binding efficiency and preparation time particularly for ELISA format [5,6] or enhancing output signals by increasing Ab concentration while limiting smears for LFIA format [7,8].

Nowadays, the well-established procedure to synthesize 10–100 nm GNPs is generally based on the reduction of the tetrachloroauric acid ($HAuCl_4$) in the presence of different concentrations of trisodium citrate as a reducing agent. [9,10]. The common highly efficient and easy-to-perform functionalization of GNPs is the conjugation by direct physical interaction of the protein with GNPs [11], based on a spontaneous absorption onto the surface of citrate stabilized nanoparticles [6].

In order to provide efficiently characterized GNP-Ab conjugates it is necessary to ensure their purification from free antibodies and on the same time to verify the GNPs-Ab stability. Last, the size and uniformity of conjugated nanoparticles needs to be addressed to achieve reproducible results.

The most common methods employed to characterize bioconjugated-GNPs are based on UV-vis spectrophotometry and transmission electron microscopy (TEM) [12,13,14]. Nonetheless, other methods, such as scanning electronic microscopy (SEM), scanning tunnelling microscopy (STM), atomic force microscopy (AFM), X-ray powder diffractometry (XRD) and Fourier transformed infrared spectroscopy (FT-IR) were also found broad application in characterization of such GNPs [15,16].

Coupled methods preceded by a separation technique can improve particle quality assurance. Size-exclusion chromatography (SEC) has been used to facilitate the characterization of GNPs [17], but its selectivity decreases when applied to higher size samples, and aspecific interactions with the stationary phase could affect GNP morphology, and determine size-dependent absorption on the packed phase. Flow field-flow fractionation (F4) represents an alternative separation technique able purify complex GNP samples, and to simultaneously offer size/spectroscopical characterization by on-line, uncorrelated detection methods[18,19]. F4 is able to separate dispersed analytes over a broad size range, from nanometer to micrometer, and the separation process is based on particle diffusion coefficient [20]. Due to the absence of a stationary phase, the separation mechanism is soft and non-invasive with total maintenance of sample properties including low strength particles interactions. F4 theory rigors are described elsewhere with applications to NPs separation [21,22]. To determine nanoparticles colloidal size, MALS is used since it allows for the determination of particle root mean square radius of gyration (Rg) by measuring the net intensity of light scattered by such particles at a range of fixed angles. The particle Rg is determined by the mass distribution within the particle [23]. F4 was online coupled with uncorrelated detection methods including multi-angle light scattering (MALS), absorbance and luminescence spectrophotometry, to achieve multidimensional characterization of NPs. F4 has been employed to size-separate GNPs [24,25], to separate proteins and NPs [26,27] and it was coupled with ICP-MS for recovery quantification [28,29].

In previous studies, F4 was online coupled to chemiluminescence (CL) detectors as a luminometer or a CCD-camera [30], demonstrating the high versatility of this technique for the non-invasive separation of protein and labelled beads. In the miniaturised version of F4, hollow fiber flow field-flow fractionation (HF5), the lower flow rate involved allows to reduce dilution of the injected sample and to increase the limit of detection. Moreover, since the cross-flow density which regulates the separation process is higher than in F4, HF5 allows to increase separation efficiency [31].

Few papers are reported about the characterization of nanoparticles and antibodies by the use of HF5 [31-36].

In this work, we propose for the first time the combined use of a miniaturized FFF, HF5, with UV-Vis absorption, fluorescence detectors and MALS (HF5-UV-FLD-MALS) to properly characterize GNP and their complex with antibodies when used as a label for LFIA.

The HF5-multidetection was used for the characterization of freshly synthesised GNPs and free antibody, for quality control of the starting materials, to evaluate the efficiency of the complex formed during conjugation of GNP and IgG, and to characterize the IgG-GNPs.

2. Materials and Methods

2.1. Chemicals

Gold(III) chloride trihydrate was purchased by Sigma Aldrich (St. Louis, MO, USA). Boric acid and NaOH were purchased from Carlo Erba (Milan, Italy). The horse-IgG antibody (produced in mouse) was kindly granted from Istituto Zooprofilattico Sperimentale dell'Abruzzo e del Molise "G. Caporale", Teramo, Italy. The mouse IgG1-FITC antibody was purchased from Sysmex, Japan.

2.2. Nanoparticle synthesis

Red GNPs were synthesised through the tetrachloroauric acid reduction using sodium citrate [10]. Briefly, a solution of chlorauric acid solution (134 µM, 95 mL) was heated to the boiling point and 5 ml. of 1% w/v sodium citrate solution was added to the boiling solution under magnetic stirring. After about a minute a greyish-blue tone appeared gradually darkening over a period of about 5 min. After 12 h of stirring at room temperature, a final colour of red wine was reached and the GNP suspension was cooled down and kept at 4°C.

2.3. Nanoparticles conjugation

The IgG-GNPs conjugate was prepared by passive adsorption of proteins onto GNPs surface, as previously described [37].

Briefly the stock solution of colloidal gold is diluted with H_2O to reach an OD ~ 1.0. to 1.0 mL of GNPs suspension, 100µLof borate buffer (20.0 mM, pH 8) were added. Then, 10.0 µL of a properly diluted antibody solution were added to obtain a final antibody concentration of 100µg/mL. The reaction mix was incubated for 30 minutes at 37 °C. Finally, to saturate functionalized GNPs surface, 100 µLof BSA 1% w/v, prepared in borate buffer (20.0 mM, pH 8), were added and the solution kept at 37 °C for 10 min. Then, the mixture was centrifuged for 10 min at 25 °C (16000 × g) and the pellet was washed first by resuspension in 1.0 mL borate buffer (20.0 mM, pH 8) with BSA 0.1% w/v, then resuspended in borate buffer (20.0 mM, pH 8) with BSA 1.0% w/v, Tween 20 0.5% v/v and finally by resuspended in borate buffer (20.0 mM, pH 8) BSA 0.1%. The conjugation reaction between antibodies and GNPs was verified by the UV-Vis spectral shift greater than 5 nm of wavelength at the maximum absorption.

In order to explore the ability to selectively detect the reacting/reacted species, we performed two different conjugations with model antibodies: one with a monoclonal anti-mouse IgG1 (IgG) and the second with a fluorescein isothiocyanate (FITC) labelled anti-mouse IgG1 (FITC-IgG).

2.4. HF5-MALS: instrumentation and method

The FFF system is composed by an HPLC with UV/Vis and fluorescence detectors connected with a module to handle FFF flows and channels.

HF5 analyses were performed using an Agilent 1200 HPLC system (Agilent Technologies, Santa Clara, CA, USA) consisting in a degasser, an isocratic pump, with an Agilent 1100 DAD UV/Vis spectrophotometer and an Agilent 1200 Fluorimeter combined with an Eclipse® DUALTEC separation system (Wyatt Technology Europe, Dernbach, Germany). The system was followed by an 18-angle multiangle light scattering detector model DAWN HELEOS (Wyatt Technology Corporation, Santa Barbara, CA, USA) The HF5 cartridge (Wyatt Technology Europe) is commercially available and has a 10kDa cutoff, a 17.5 cm length, a 0.8mm diameter for an internal volume of 90µL. The scheme of the HF5 cartridge, its assembly and the modes of operation of the Eclipse® DUALTEC system have already been described elsewhere [38]. ChemStation version B.04.02 (Agilent Technologies) data system for Agilent instrumentation was used to set and control the instrumentation and for the computation of various separation parameters, complete with the Wyatt Eclipse @ ChemStation version 3.5.02 (Wyatt Technology Europe). ASTRA® software version 6.1.7 (Wyatt Technology Corporation) was used to handle signals from the detectors (MALS and UV) and to compute radius and molar mass of particles.

The separation mechanism has been previously reported [39]; flow conditions for the HF5 method are reported in Table 1.

After samples injection in the HF5 fiber, the separation process is performed in four steps: (1) *Focus*. During focus a flow of mobile phase is split into two different streams entering from inlet and outlet. This step is used to stabilize flows. (2) *Focus–injection*, the flow settings remain unvaried. The sample is introduced into the channel through the inlet and the flow settings allows to focus analytes in a narrow band at the begging of separation channel. (3) *Elution*. After sample injection, the flow settings change and a flow of mobile phase enters the channel only by the inlet. Part of it comes out transversely through the channel pores (cross-flow), while the rest (channel flow, Vc) reaches the detectors. The strength of hydrodynamic field applied to nanoparticles for their separation can be

regulated by modifying the intensity of cross-flow while analytes elute along the fiber towards the detectors. This parameter can be modified throughout the analysis to generate a decreasing cross-flow (namely gradient). (4) *Elution–injection*. The cross-flow is set to zero and the mobile phase flows along the fiber to the detectors allowing for any remaining sample due to the cross-flow action inside the channel to be released. Also, the flow is redirected in the injection line as well to clean it before the next injection.

The separation method was used to analyze GNPs (50µL of a 0.5 OD solution injected), BSA (50 µg injected), IgG (50µg injected), FITC-IgG (40µg injected), and the two conjugates IgG-GNP and FITC-IgG-GNP (50µL of a 0.5 OD solution injected for each sample). All analyses were carried out in borate buffer (20 mM, pH8) as mobile phase. Reproducibility was optimal and sample recovery after focusing was >94% for all samples.

Table 1. Flow conditions for HF5 analyses of reagents and conjugated GNPs. Longitudinal flow is indicated as Vc, while cross/focus flow as Vx.

Focus (mL/min)	Focus-injection (mL/min)	Elution (mL/min)	Elution (mL/min)	Elution (mL/min)	Elution (mL/min)	Elution (mL/min)	Elution-Inject (mL/min)
Vx = 0.8 T= 0.5 min	Vx = 0.8 T= 3 min	Vx= 0.4 T= 4 min	Vx= 0.4 to 0.1 T= 4 min	Vx= 0.1 to 0.03 T= 4 min	Vx= 0.03 T= 10 min	Vx= 0.00 T= 2 min	Vx= 0.00 T= 2 min

The particle retention is a function of its apparent diffusion coefficient, and consequently, to hydrodynamic diameter (*D*h) or radius (*R*h). Due to the parabolic flow profile of the carrier flow, smaller particles experience higher flow rates (on the average) than larger ones. To determine nanoparticles colloidal size, MALS is used since it allows for the determination of particle root mean square radius of gyration (Rg) by measuring the net intensity of light scattered by such particles at a range of fixed angles. The particle Rg is determined by the mass distribution within the particle. The Zimm approximation was used to fit scattering data. The single mass increments are weighed by the square of the radius distance from the center of mass. Consequently, two particles with same

hydrodynamic radius (Rh), but with different Rg values, may have a different mass distribution, and thus, different shapes

3. Results and discussion

There are three critical issues of a new GNP-conjugate to be used for LFIA: i. synthesis of nanoparticles, where the quality of GNP has to be controlled; ii. during conjugation, when it is essential to verify the effective conjugation, and iii. after conjugation, when the purification and characterization of the (FITC)IgG-GNP conjugate is to be performed.

Hence, in order to develop an HF5 method protocol we follow, the experimental approach schematized in Figure 1. First, the HF5 method should allow an analysis of reagents involved in NPs synthesis and conjugation (step a, Figure 1): the HF5 method must be able to achieve an adequate resolution with different retention time for GNPs and IgG in a short analysis time; on-line orthogonal multidetection provides specific signals for each species. Then, after the conjugation reaction, the product obtained together with supernatants were analyzed in order to verify the effective conjugation. The analysis of supernatant allows the determination of the presence/absence of unreacted IgG and to recover IgG (step b, Figure 1); while the analysis of resuspended precipitate allows to isolate and characterize IgG-GNPs conjugate and to verify its stability (step c, Figure 1).

3.1. HF5-multidetection pre-conjugation: characterization of reagents

To characterize reagents involved in the conjugation reaction, diagnostic signals for IgG and GNPs, together with BSA used for NPs saturation, should be evaluated. BSA and IgG are both proteins and absorb in the UV with a wavelength maximum at 280 nm. However, GNPs also absorb at that wavelength and the signal cannot be used to uniquely attribute peaks. Proteins though also display intrinsic fluorescence (emission at 340 nm upon excitation at 280 nm) whereas GNP do not: this is the detection of choice for BSA and IgG. the conjugate FITC-IgG is also protein, hence could be detected at 340 nm as well, in addition it has the unique fluorescent emission at 518 nm (upon excitation at 490) due to FITC moiety and therefore this is the diagnostic signal we chose. Last, the 530 nm absorption is peculiar for GNPs and was used to recognize the peaks corresponding to gold particles of the used size.

The HF5 separative method employed a combination of decreasing cross flow rates (Table 1), to have BSA (66.4 kDa) be resolved from IgGs (about 180 kDa) but also to reduce the analysis time as much

as possible to avoid excessive dilution of GNPs. The results obtained from the optimized method applied to single injections of all reagents are shown in Figure 2. All analyses are carried out in borate buffer to facilitate GNP suspension and can be performed in less than 30 minutes.

BSA is eluted in a single sharp peak at 6.5 minutes (Figure 2a), with no overlap with IgGs which are eluted at around 11 minutes (Figure 2b for IgG and 2c for FITC-labelled IgG respectively). Finally, GNPs are only eluted when the crossflow is very low, i.e. after 14 minutes, and display a broad band peaking at 17.5 min (Figure 2d), as a result of bigger hydrodynamic radius with a consequent broader size distribution. The in-depth size characterization of the starting GNPs will be discussed in Section 2.4 together with the conjugates' one.

A summarizing scheme of these results is shown in Figure 2e, where all peaks are represented on the same timeline to highlight the achieved separation: if all these species are present in the same mixture, they would all be selectively detected with the right detection wavelengths without controversies.

3.2. HF5-multidetection mid and post-conjugation: Analysis of supernatants and IgG-GNP products

After the analysis of single reagents with the HF5 method, we followed the conjugation protocol and incubated GNPs with IgG or FITC-IgG, then saturated with BSA and centrifuged to precipitate the conjugate; then we tested the method for the analysis of supernatants (step b, Figure 1) and analysis of precipitates/products (step c, Figure 1).

The fractograms obtained from the analysis of the two supernatants (derived from IgG and FITC-IgG conjugation, respectively) are shown in Figure 3a and 3b; while the analysis of products are reported in Figure 3c and 3d.

The supernatants should contain either BSA, in the case of a successful quantitative conjugation with IgGs, or BSA and unreacted conjugant if IgGs were in excess or the reaction was unsuccessful. Figure 3a, shows that BSA (light grey line, peaking at 7 min), is the only species present in suspension. There is no signal at 530 nm corresponding to GNPs, dark grey line) and at the retention time of IgG (~11 min) the typical fluorescence signal is flat (red dotted selection).

Likewise, in Figure 3b we see how BSA is the only emitting species, while both GNP absorption and FITC-IgG specific fluorescence signals are absent (dark grey and green lines, respectively).

Subsequently, the precipitated, washed, and resuspended GNP conjugates were analysed with the same method and the results are shown in Figure 3c (conjugaton using IgG) and 3d (conjugation using

FITC-IgG). Since the intrinsic or specific fluorescence of these proteins/labelled proteins would be quenched by GNPs [40,41], the diagnostic signals relative to IgG and IgG-FITC cannot be expected on the nanoparticles, and to check for effective functionalisation it is necessary to determine conjugation "by absence", as demonstrated by the lack of signal due to free IgG.

From the HF5 analysis (Figure 3 c and d), BSA is present at its characteristic retention time (~6 min), since it is also added in the resuspension buffer (0.1%). The signal corresponds to about 50µgof BSA injected as expected, and it is similar for the two conjugates since they underwent the same protocol. In both conjugates there is no release of IgG conjugant (no signal in correspondence of the red or green square, ~11 min). These results confirm a quantitative conjugation between antibody added and GNPs. Conjugated GNPs are then eluted in a broad band with a maximum at t~19 min. These retention bands show a different intensity and peak shape, indicating that the nature of the IgG (such as the presence of hydrophobic dyes) reflects on particle stability in suspension and on the possible insurgence of particle-particle interactions.

3.3. Size and spectral characterization of GNPs and (FITC)-IgG-GNPs

The combination of a photodiode array (PDA) UV-Vis detector and MALS also provide spectral and size information, to fully characterize the GNP conjugates.

The radius distribution and the absorption spectrum for GNPs, IgG-GNPs and FITC-IgG-GNPs are shown in Figure 4. Since the UV-Vis absorption spectra are collected over the peak elution time, the result is a 3D image where the axes are intensity, wavelength and time.

The synthesized GNPs show a monomodal distribution, which averages at 20 ± 4 nm, in agreement with what expected from the synthesis condition. When conjugated, the gyration radius increases differently depending on the type of IgG used. For what concerns IgG-GNPs, the radius increases to 33 ± 4 nm, while for FITC-IgG-GNPs the radius increases further to 53 ± 7 nm. Fluorescein is a small molecule and its addition onto the IgG should not sensibly increase the protein size. However, the radius increase due to the presence of the dye is index of the onset of hydrophobic interactions between dye molecules which reduce solubility and promote surface interactions between particles.

This is a further confirmation that the two conjugation procedures were successful, since two different nanoparticle populations were generated, and the only difference in the protocol was the different conjugant employed. A comparison of the size measured for the unconjugated and conjugated nanoparticles show that they are statistically different ($p<0.0001$) indicating that the original

nanoparticles are not present anymore. This estimation suggests that all GNPs have interacted with the conjugants and gives insight on the stoichiometry of the conjugation. Last, this approach can be expanded towards the understanding of conjugation stoichiometry. Since the combination of information from steps b and c (Figure 1) allows to detect and recover unreacted conjugant, a loading study of GNP with increasing amounts of IgG can be promptly set up with low volume requirements. Simultaneously, the conjugated-GNP quality would be assessed with the online characterization to obtain the highest-loaded and most stable conjugate.

Moreover it is possible to notice how absorption increases for IgG-GNPs with respect to GNPs, which is both an index of a higher extinction due to particle size and of an increased stability in suspension for the stabilizing effect of a protein coating [42].

On the other side, the absorption is lower for FITC-IgG-GNPs where the hydrophobic contribution of the fluorescent dye hinders stability: only the suspension-stable particles reach the detectors and can be collected. If on one side this is a disadvantage given the loss of material, on the other the HF5 separation process allows to recover the most stable conjugates even when the conjugation is difficult and sub-optimal.

In Figure 4 (d, e, f respectively) the UV absorption spectra are also shown for each population: they allow verifying that the entire peak has the same absorption pattern (the populations are each uniform in composition). Unconjugated and IgG-conjugated nanoparticles show a similar spectrum, thought IgG-GNPs have a red shift.

FITC-IgG-GNPs had a more distinctive spectrum, with broader maxima also shifter further towards higher wavelengths, reflecting the size-dependent shift in the surface plasmon resonance

3.4. Comparison with conventional characterisation tools

Last, we wanted to evaluate the characterization results in terms of surface plasmon resonance (SPR) attribution. In fact, UV-Vis characterisation of synthesized and conjugated nanoparticles is often the main (or only) technique used to verify the correct size of GNPs prior to further application. After GNP synthesis and conjugation, we also recorded the UV-Vis spectrum for all three species with a batch spectrophotometer, and the three profiles are overlaid in Figure 5a. In Figure 5b, the spectra obtained at peak maximum of the HF5 separation are instead shown. The SPR value for GNPs was found to be 530 and 526 nm, respectively: the latter is more in agreement with a size of 20 nm, as determined from MALS calculation. On the opposite, the SPR maxima found for IgG and FITC-IgG

conjugates are at a higher wavelength for HF5-purified particles than what obtained batch analyses: from 535 to 540 nm for IgG-GNPs and from 541 to 552 nm for FITC-IgG-GNPs. In both cases, the values measured from HF5 fractionation result more compatible with the measured radii of 30 and 53 nm [42]. Moreover, the peaks are sharper, since there is no interference from other species and BSA cannot act as non-covalent surfactant, masking the real size of NPs. In conclusion, while UV batch characterization is fundamental as a fast check for synthesis and conjugation, a more accurate estimation of GNPs/conjugated GNPs nanoparticles through HF5 analysis is also desirable and beneficial to enhance accuracy.

4. Conclusions

The availability of pure, homogeneous and well characterized bioconjugated gold nanoparticles, is crucial to ensure the fast and efficient development of new immunosensors. To support their production and provide reliable data, we exploited an analytical platform based on HF5 separation and equipped with UV absorption and fluorescence, together with multi-angle light scattering.

The HF5 approach helped checking for the actual formation of a FITC-IgG-GNP conjugate with fundamental information on GNP size, conjugation success, and conjugate properties in less than 30 minutes for each analysis.

Moreover, through size and spectral characterization, we correlated each nanoparticle population with their size and surface plasmon resonance shift, with more accuracy than current routine techniques. Last, the baseline resolution obtained between each species gives chance to recollect unreacted conjugants or purified nanoparticles for immediate application or further testing.

In perspective before the HF5 method can be used as quality control even before performing the washing and centrifugation steps, and it could be useful in shortening the development phase by cutting the last purification and reconcentration steps when unnecessary (there is no leftover IgG) or when the conjugation is not successful, and allowing to repeat the experiment with improved strategies. This approach offers the chance of collecting purified fractions for immediate use or further testing.

Acknowledgements

We would like to acknowledge and thank Professor Aldo Roda, who endorsed this collaboration and offered many interesting insights on research ideas and directions.

Competing interests

Valentina Marassi, Andrea Zattoni, Pierluigi Reschiglian and Barbara Roda are associates of the academic spinoff company byFlow Srl (Bologna, Italy). The company mission includes know-how transfer, development, and application of novel technologies and methodologies for the analysis and characterization of samples of nano-biotechnological interest.

Figures captions

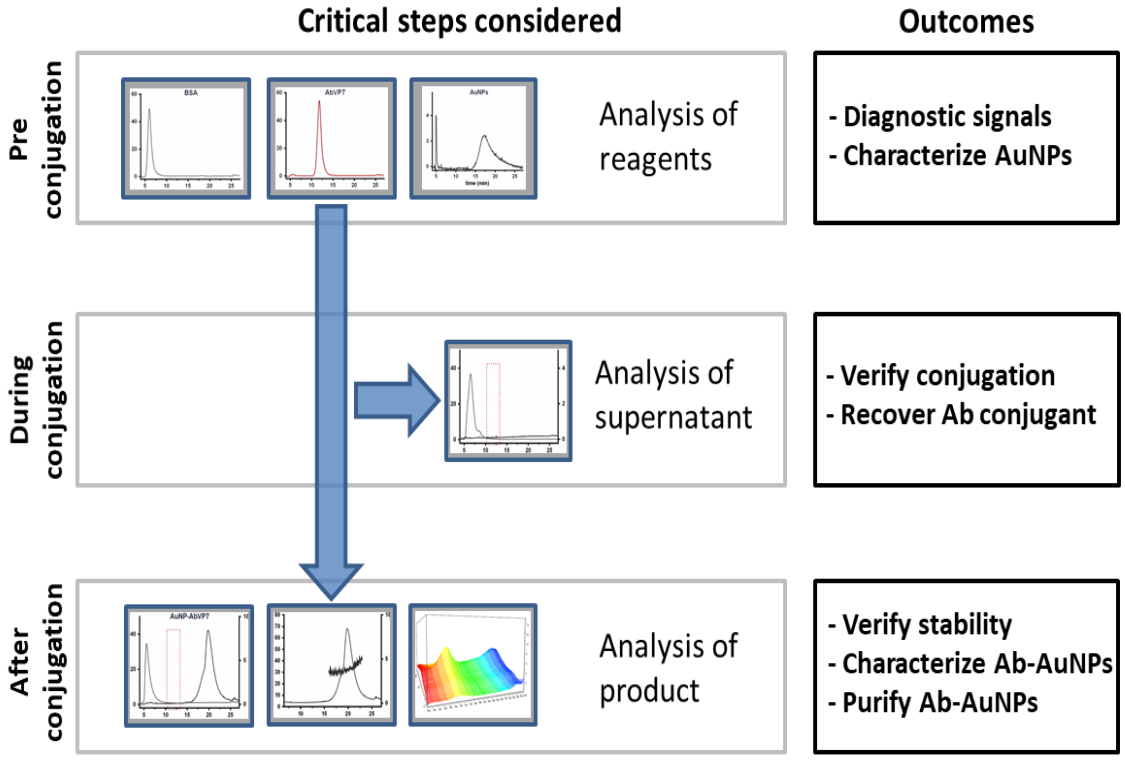

Figure 1: schematic representation of the analytical approach used in this work.

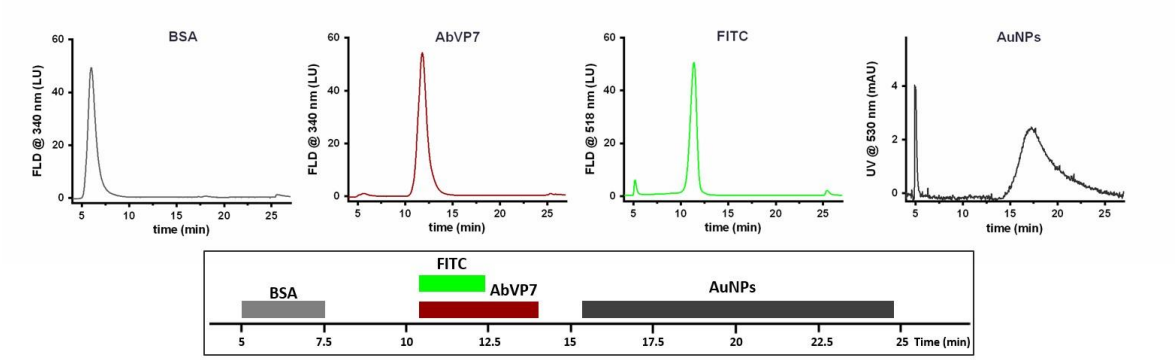

Figure 2: fractograms obtained from HF5-UV-FLD analysis of all reagents used in the conjugation protocol and detected with their diagnostic signal. a) BSA, fluorescence (ex 280 nm, em 340 nm). b) IgG, (ex 280 nm, em 340 nm). c) FITC-IgG, (ex 490 nm, em 518 nm). d) freshly synthesized GNPs, (absorption at 530 nm). e) schematization of all elution times overlaid within the same runtime.

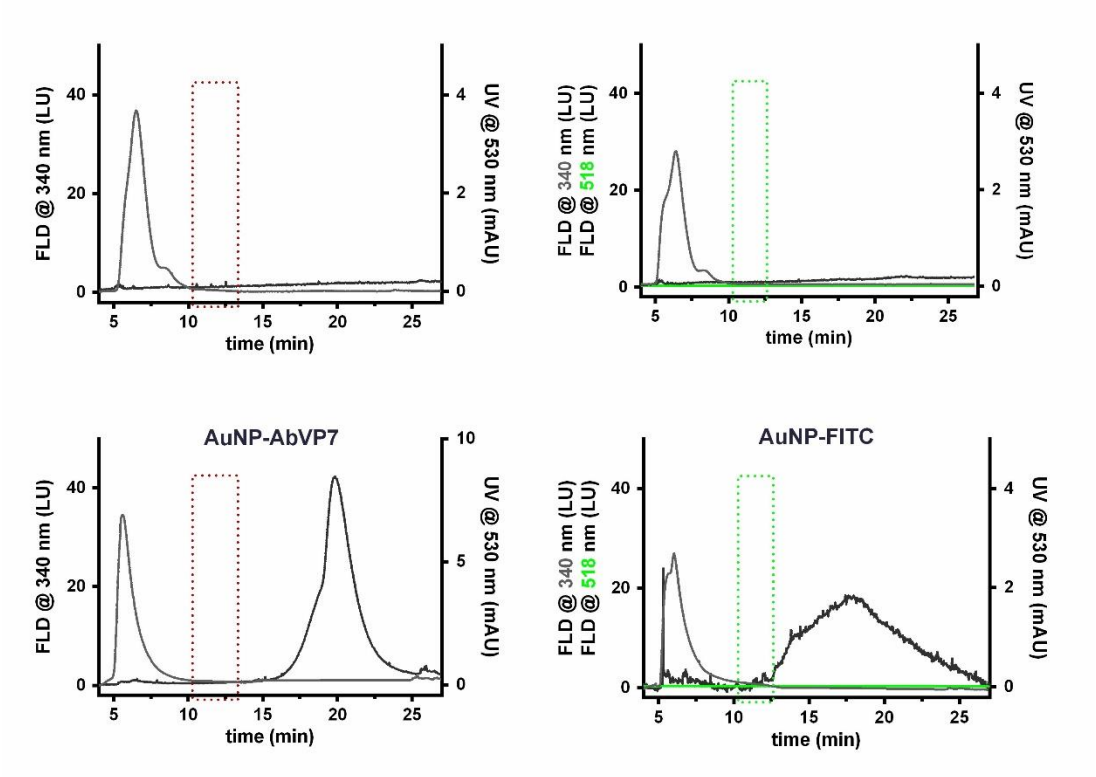

Figure 3: fractograms obtained from the analyses of supernatants and products. a) supernatant from IgG-GNP conjugation. b) supernatant from FITC-IgG-GNP conjugation. Red and green dotted squares: absence of conjugant at the expected retention time. c) fractogram of IgG-GNPs at diagnostic

wavelengths for each species. d) fractogram of FITC-IgG-GNPs at diagnostic wavelengths for each species.

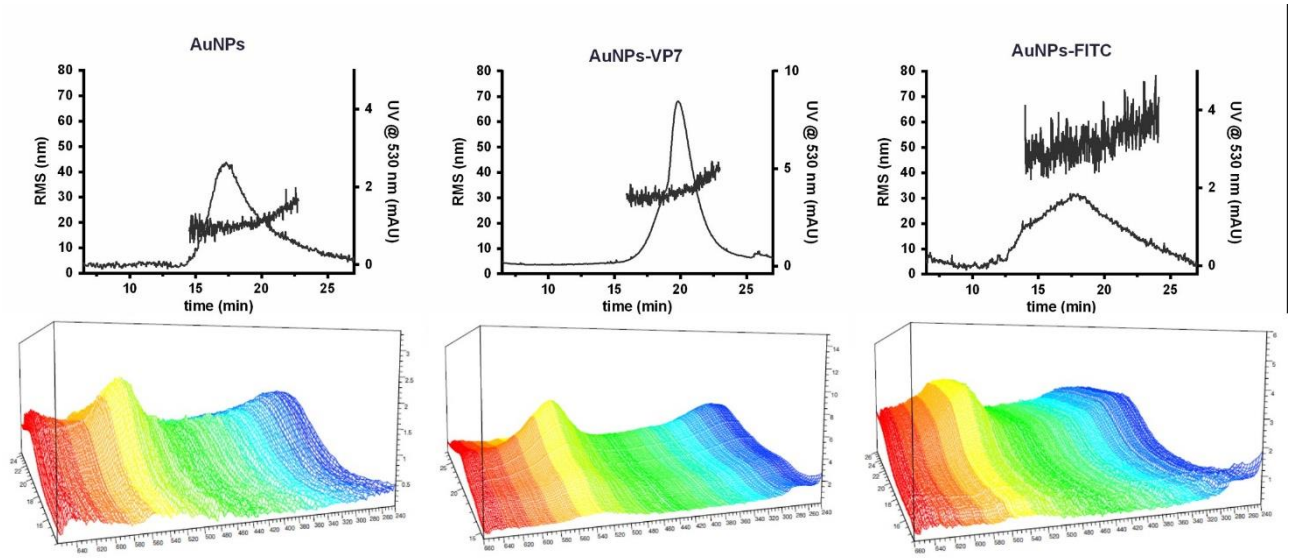

Figure 4: Radius distribution of GNPs (a), IgG-GNPs (b) and FITC-IgG-GNPs (c). 3D absorption spectrum recorded for GNPs (d), IgG-GNPs (e), and FITC-IgG-GNPs (f).

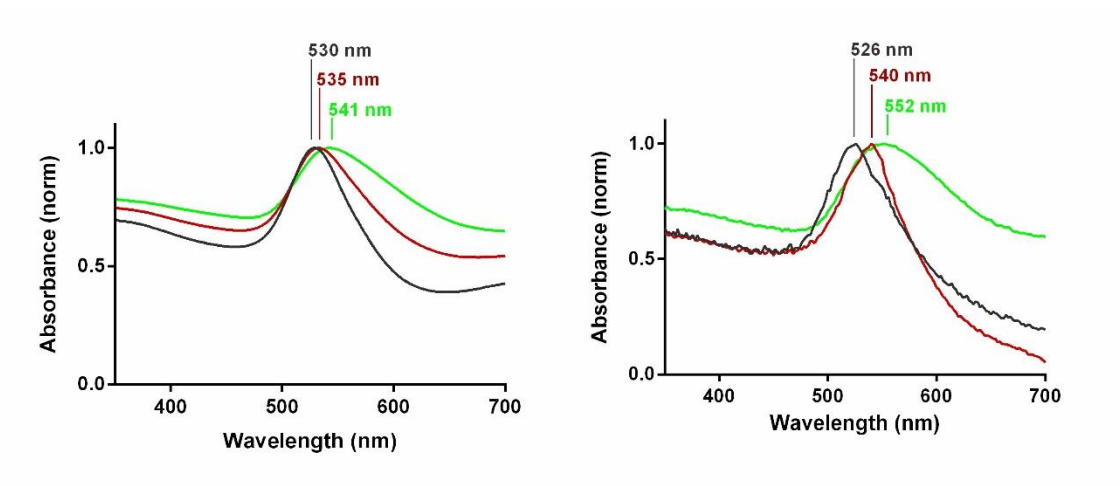

Figure 5: UV-Vis absorption spectrum of gold nanoparticles obtained (a) with batch measurement and (b) from HF5-separated peaks. grey: GNPs. Red: IgG-GNPs. Green: FITC-IgG-GNPs.

References

[1] B.D. Chithrani, W.C.W. Chan. Elucidating the mechanism of cellular uptake and removal of protein-coated gold nanoparticles of different sizes and shapes. Nano Lett. 7 (2007) 1542-1550. https://doi.org/10.1021/nl070363y.

[2] Y. Xia, W. Li, C.M. Cobley, J. Chen, X. Xia, Q. Zhang, E.C. Cho, P.K. Brown. Gold nanocages: from synthesis to theranostic applications. Acc. Chem. Res. 44 (2011) 914-24. https://doi.org/10.1021/ar200061q.

[3] C.J. Murphy, A.M. Gole, J.W. Stone, P.N. Sisco, A.M. Alkilani, E.C. Goldsmith, S.C. Baxter. Gold nanoparticles in biology: beyond toxicity to cellular imaging. Acc. Chem. Res. 41 (2008) 1721-1730. https://doi.org/10.1021/ar800035u.

[4] A.M. Alkilany, S.E. Lohse, C.J. Murphy. The gold standard: gold nanoparticle libraries to understand the nano-bio interface. Acc. Chem. Res. 46 (2013) 650-661. https://doi.org/10.1021/ar300015b.

[5] R. Huang, K. Zhang, G. Zhu, Z. Sun, S. He, W. Chen. Blocking-Free ELISA using a gold nanoparticle layer coated commercial microwell plate. Sensors. 18.10 (2018) 3537. https://doi.org/10.3390/s18103537.

[6] P. Ciaurriz, F. Fernández, E. Tellechea, J.F. Moran, A.C. Asensio. Comparison of four functionalization methods of gold nanoparticles for enhancing the enzyme-linked immunosorbent assay (ELISA). Beilstein J. Nanotechnol. 8.1 (2017) 244-253. https://doi:10.3762/bjnano.8.27.

[7] A.L. Tomás, M.P. De Almeida, F. Cardoso, M. Pinto, E. Pereira, R. Franco, O. Matos. Development of a Gold Nanoparticle-Based Lateral-Flow Immunoassay for Pneumocystis Pneumonia Serological Diagnosis at Point-of-Care. Front. Microbiol. 10 (2019) 2917. https://doi.org/10.3389/fmicb.2019.02917.

[8] R. Pan, Y. Jiang, L. Sun, R. Wang, K. Zhuang, Y. Zhao, W. Hui, Md. A. Aslam, Honghua Xu, Man, C. Gold nanoparticle-based enhanced lateral flow immunoassay for detection of Cronobacter sakazakii in powdered infant formula. J. Dairy Sci. 101.5 (2018) 3835-3843. https://doi.org/10.3168/jds.2017-14265.

[9] J. Turkevich, G. Kim. Palladium: preparation and catalytic properties of particles of uniform size. Science, 169.3948 (1970) 873-879. https://10.1126/science.169.3948.873.

[10] J. Turkevich, P.C. Stevenson, J. Hillier. A study of the nucleation and growth processes in the synthesis of colloidal gold. Discuss Faraday Soc. 11.0 (1951) 55–75. https://doi.org/10.1039/DF9511100055.

[11] Y. Zhao, G. Zhang, Q. Liu, M. Teng, J. Yang, J. Wang. Development of a lateral flow colloidal gold immunoassay strip for the rapid detection of enrofloxacin residues. J. Agric. Food Chem. 56.24 (2008) 12138-12142. https://pubs.acs.org/doi/pdf/10.1021/jf802648z

[12] P. Ciaurriz, F. Fernández, E. Tellechea, J.F. Moran, A.C. Asensio. Comparison of four functionalization methods of gold nanoparticles for enhancing the enzyme-linked immunosorbent assay (ELISA). Beilstein J. Nanotechnol. *8*.1 (2017) 244-253. http://doi:10.3762/bjnano.8.27.

[13] E. Colangelo, J. Comenge, D. Paramelle, M. Volk, Q. Chen, R. Levy. Characterizing Self-Assembled Monolayers on Gold Nanoparticles. Bioconjugate Chem. 28 (2017) 11–22. https://doi.org/10.1021/acs.bioconjchem.6b00587.

[14] J.P. Lata, L. Gao, C. Mukai, R. Cohen, J.L. Nelson, L. Anguish, S. Coonrod, A.J. Travis. Effects of Nanoparticle Size on Multilayer Formation and Kinetics of Tethered Enzymes. Bioconjugate Chem. 26.9 (2015) 1931–1938. https://doi.org/10.1021/acs.bioconjchem.5b00354.

[15] M.T. Castan˜eda, S. Alegret, A. Merkoci. Electrochemical Sensing of DNA Using Gold Nanoparticles. Electroanalysis. 19.7–8 (2007) 743–753. https://doi.org/10.1002/elan.200603784.

[16] S. Guo, E. Wang. Synthesis and electrochemical applications of gold nanoparticles. Anal. Chim. Acta 598.2 (2007) 181–192. https://doi.org/10.1016/j.aca.2007.07.054.

[17] L. Pitkänen, A.M. Striegel. Size-exclusion chromatography of metal nanoparticles and quantum dots. TrAC Trends Analyt. Chem. 80 (2016) 311-320. https://doi.org/10.1016/j.trac.2015.06.013.

[18] C. Contado. Field flow fractionation techniques to explore the "nano-world". Anal. Bioanal. Chem. 409.10 (2017) 2501-2518. https://doi.10.1007/s00216-017-0180-6.

[19] A. Zattoni, B. Roda, F. Borghi, V. Marassi, P. Reschiglian. Flow field-flow fractionation for the analysis of nanoparticles used in drug delivery. J. Pharm. Biomed. Anal. 87 (2014) 53-61. https://doi.org/10.1016/j.jpba.2013.08.018.

[20] J.C. Giddings. Field-flow fractionation: analysis of macromolecular, colloidal, and particulate materials. Science. 260 (1993) 1456–1465. https://doi.10.1126/science.8502990.

[21] R. Beckett, Z. Jue, C. Giddings. Determination of molecular weight distributions of fulvic and humic acids using flow field-flow fractionation. Environ. Sci. Technol. 21 (1987) 289.

[22] M. Marioli, W.T. Kok. Continuous asymmetrical flow field-flow fractionation for the purification of proteins and nanoparticles. Separation and Purification Technology. 242 (2020) 116744. https://doi.org/10.1016/j.seppur.2020.116744.[23] V. Marassi, B. Roda, S. Casolari, S. Ortelli, M. Blosi, A. Zattoni, A.L. Costa, P. Reschiglian. Hollow-fiber flow field-flow fractionation and multi-

angle light scattering as a new analytical solution for quality control in pharmaceutical nanotechnology. Microchem. J., 136 (2018) 149-156. https://doi.org/10.1016/j.microc.2016.12.015.
[24] B. Meisterjahn, S. Wagner, F. von der Kammer, D. Hennecke, T. Hofmann. Silver and gold nanoparticle separation using asymmetrical flow-field flow fractionation: influence of run conditions and of particle and membrane charges. J. Chromatogr. A. 1440 (2016) 150-159. https://doi.org/10.1016/j.chroma.2016.02.059.
[25] I. V.Safenkova, E. S.Slutskaya, V. G.P anferov, A. V. Zherdev, B B.Dzantiev. Complex analysis of concentrated antibody-gold nanoparticle conjugates' mixtures using asymmetric flow field-flow fractionation. J. Chromatogr. A. 1477 (2016) 56-63. https://doi.org/10.1016/j.chroma.2016.11.040
[26] R. Saenmuangchin, A. Siripinyanond, Flow field-flow fractionation for hydrodynamic diameter estimation of gold nanoparticles with various types of surface coatings. Anal Bioanal Chem. 410 (2018) 6845–6859. https://doi.org/10.1007/s00216-018-1284-3
[27] J. Ashby, S. Schachermeyer, S. Pan, W. Zhong. Dissociation-Based Screening of Nanoparticle-Protein Interaction via Flow Field-Flow Fractionation. Anal Chem. 85-15 (2013) 7494–7501. https://doi.org/10.1021/ac401485j.
[28] B. Schmidt, K. Loeschner, N. Hadrup, A. Mortensen, J.J. Sloth, C. Bender Koch, E.H. Larsen. Quantitative characterization of gold nanoparticles by field-flow fractionation coupled online with light scattering detection and inductively coupled plasma mass spectrometry. Anal. Chem. 83.7 (2011) 2461-2468. https://doi.org/10.1021/ac102545e.
[29] E.P. Gray, T.A. Bruton, C.P. Higgins, R.U. Halden, P. Westerhoff, J.F. Ranville. Analysis of gold nanoparticle mixtures: a comparison of hydrodynamic chromatography (HDC) and asymmetrical flow field-flow fractionation (AF4) coupled to ICP-MS. J. Anal. At. Spectrom. 27.9 (2012) 1532-1539. https://doi.10.1039/C2JA30069A.
[30] D. Melucci, M. Guardigli, B. Roda, A. Zattoni, P. Reschiglian, A. Roda. A new method for immunoassays using field-flow fractionation with on-line, continuous chemiluminescence detection. Talanta. 60.2-3 (2003) 303-312. https://doi.org/10.1016/S0039-9140(03)00106-1.
[31] V. Marassi, S. Casolari, B. Roda, A. Zattoni, P. Reschiglian, S. Panzavolta, S.A.M. Tofail, S. Ortelli, C. Delpivo, M. Blosi, A.L. Costa. Hollow-fiber flow field-flow fractionation and multi-angle light scattering investigation of the size, shape and metal-release of silver nanoparticles in aqueous medium for nano-risk assessment. J. Pharm. Biomed. Anal. 106 (2015) 92-99. https://doi.org/10.1016/j.jpba.2014.11.031.

[32] P. Reschiglian, B. Roda, A. Zattoni, M. Tanase, V. Marassi, S. Serani. Hollow-fiber flow field-flow fractionation with multi-angle laser scattering detection for aggregation studies of therapeutic proteins. Anal. Bioanal. Chem., 406.6 (2014) 1619-1627. https://doi.org/10.1007/s00216-013-7462-4.

[33] Z.Q. Tan, J.F. Liu, X.R. Guo, Y.G. Yin, S.K. Byeon, M.H. Moon, G.B. Jiang. Toward Full Spectrum Speciation of Silver Nanoparticles and Ionic Silver by On-Line Coupling of Hollow Fiber Flow Field-Flow Fractionation and Minicolumn Concentration with Multiple Detectors. Anal. Chem. 87.16 (2015) 8441-8447. https://doi.org/10.1021/acs.analchem.5b01827.

[34] R. Saenmuangchin, J. Mettakoonpitak, J. Shiowatana, A. Siripinyanond. Separation of silver nanoparticles by hollow fiber flow field-flow fractionation: Addition of tannic acid into carrier liquid as a modifier. J. Chromatogr. A. 1415 (2015) 115-122. https://doi.org/10.1016/j.chroma.2015.08.047

[35] M. Blosi, S. Albonetti, M. Dondi, G. Baldi, A. Barzanti, M. Bitossi. Process for preparing stable suspensions of metal nanoparticles and the stable colloidal suspensions obtained thereby. Google Patents: 2011.

[36] S. Dubascoux, F. Von Der Kammer, I. Le Hécho, M.P. Gautier, G. Lespes. Optimisation of asymmetrical flow field flow fractionation for environmental nanoparticles separation. J. Chromatogr. A. 1206.2 (2008) 160-165. https://doi.org/10.1016/j.chroma.2008.07.032.

[37] F. Di Nardo, C. Baggiani, C. Giovannoli, G. Spano, L. Anfossi. Multicolor immunochromatographic strip test based on gold nanoparticles for the determination of aflatoxin B1 and fumonisins. Microchim. Acta 184 (2017) 1295–1304. https://doi.10.1007/s00604-017-2121-7.

[38] P. Reschiglian, A. Zattoni, L. Cinque, B. Roda, F. Dal Piaz, A. Roda, M.H. Moon, B.R. Min. On-Line Hollow-Fiber Flow Field-Flow Fractionation-Electrospray Ionization/Time-of-Flight Mass Spectrometry of Intact Proteins. Anal. Chem. 76 (2004) 2103-2111. https://doi.org/10.1021/ac048898o.

[39] P. Reschiglian, A. Zattoni, B. Roda, D.C. Rambaldi, M.H. Moon. Hollow-Fiber Flow Field-Flow Fractionation: A Pipeline to Scale Down Separation and Enhance Detection of Proteins and Cells, in Field-Flow Fractionation in Biopolymer Analysis. S.K.R. Williams and K.D. Caldwell, Editors. 2012, Springer Vienna: Vienna. p. 37-55. https://doi.org/10.1007/978-3-7091-0154-4_3.

[40] B. Dubertret, M. Calame, A.J. Libchaber. Single-mismatch detection using gold-quenched fluorescent oligonucleotides. Nat. Biotechnol., 19.4 (2001) 365-370. https://doi.org/10.1038/86762.

[41] L. Ao, F. Gao, B. Pan, R. He, D. Cui. Fluoroimmunoassay for antigen based on fluorescence quenching signal of gold nanoparticles. Anal. Chem. 78.4 (2006) 1104-1106. https://doi.org/10.1021/ac051323m.

[42] P.K. Jain, K.S. Lee, I.H. El-Sayed, M.A. El-Sayed. Calculated absorption and scattering properties of gold nanoparticles of different size, shape, and composition: applications in biological imaging and biomedicine. J. Phys. Chem. B. 110.14 (2006) 7238-7248. https://doi.org/10.1021/jp057170o.